

See discussions, stats, and author profiles for this publication at: <https://www.researchgate.net/publication/266382940>

# Improved Characterization of Slow-Moving Landslides by means of Adaptive NL-InSAR Filtering

Conference Paper *in* Proceedings of SPIE - The International Society for Optical Engineering · September 2014

DOI: 10.1117/12.2067357

---

CITATIONS

2

READS

151

4 authors, including:



Rubén Iglesias  
Dares Technology

48 PUBLICATIONS 458 CITATIONS

[SEE PROFILE](#)



Ciscu Sánchez  
TRE-ALTAMIRA, Spain

15 PUBLICATIONS 52 CITATIONS

[SEE PROFILE](#)



Javier Duro  
Altamira Information

39 PUBLICATIONS 552 CITATIONS

[SEE PROFILE](#)

# Improved Characterization of Slow-Moving Landslides by means of Adaptive NL-InSAR Filtering

David Albiol, Rubén Iglesias, Francisco Sánchez and Javier Duro  
Altamira-Information, C/ Còrsega, 381-387, E-08037, Barcelona (Spain).

## ABSTRACT

Advanced remote sensing techniques based on space-borne Synthetic Aperture Radar (SAR) have been developed during the last decade showing their applicability for the monitoring of surface displacements in landslide areas. This paper presents an advanced Persistent Scatterer Interferometry (PSI) processing based on the Stable Point Network (SPN) technique, developed by the company Altamira-Information, for the monitoring of an active slow-moving landslide in the mountainous environment of *El Portalet*, Central Spanish Pyrenees. For this purpose, two TerraSAR-X data sets acquired in ascending mode corresponding to the period from April to November 2011, and from August to November 2013, respectively, are employed. The objective of this work is twofold. On the one hand, the benefits of employing Nonlocal Interferometric SAR (NL-InSAR) adaptive filtering techniques over vegetated scenarios to maximize the chances of detecting natural distributed scatterers, such as bare or rocky areas, and deterministic point-like scatterers, such as man-made structures or poles, is put forward. In this context, the final PSI displacement maps retrieved with the proposed filtering technique are compared in terms of pixels' density and quality with classical PSI, showing a significant improvement. On the other hand, since SAR systems are only sensitive to detect displacements in the line-of-sight (LOS) direction, the importance of projecting the PSI displacement results retrieved along the steepest gradient of the terrain slope is discussed. The improvements presented in this paper are particularly interesting in these type of applications since they clearly allow to better determine the extension and dynamics of complex landslide phenomena.

**Keywords:** InSAR, DInSAR, PSI, SPN, Nonlocal InSAR, Landslide Monitoring, Down-slope projection

## 1. INTRODUCTION

Synthetic Aperture Radar (SAR) data allow obtaining all-day all-weather reflectivity images of large-scale areas of observation. If SAR images are acquired at different temporal instants, Differential SAR Interferometry (DInSAR) techniques allow the exploitation of the interferometric phase, i.e., the phase-differences between SAR pairs, in order to retrieve ground displacement information with millimetric accuracy [1]. Nonetheless, the exploitation of the interferometric phase becomes complex as the temporal baseline of the interferometric pairs becomes larger, or under the presence of hard atmospheric artifacts.

In order to overcome these limitations, different Persistent Scatterer Interferometry (PSI) techniques have been developed during the last decade [2–15]. In that case, larger data sets of SAR images are employed to fix multi-temporal phase relationships between the different SAR acquisitions available. PSI techniques allow the estimation of both the linear and the non-linear components of the ground displacement produced in the area of observation, as well as the Atmospheric Phase Screen (APS) for each SAR acquisition. Nowadays, there exist a lot of applications showing their applicability for monitoring complex ground displacement episodes. Examples of such applications include the modeling of subsidence and/or uplift phenomena in urban environments [6], glaciers monitoring [16], landslides' characterization [17], soil compaction rate computation [18] or atmosphere estimation [19].

Among all these applications, the accurate monitoring of landslides is becoming one of the most interesting issues in the remote sensing community. This topic has been traditionally addressed with the employment of geotechnical devices, such as inclinometers, extensometers, piezometers, or Differential Global Positioning System (DGPS) networks. In general, these in-field techniques provide poor densities and a lower extent compared with

---

Further author information: (Send correspondence to J.D.)

J.D.: E-mail: javier.duro@altamira-information.com, Telephone: +34 93 183 57 50

SAR sensors. Furthermore, they require the direct installation of devices over the landslide surface, which may be a complex task when the accessibility to the area of interest is limited. The development of remote sensing tools based on space-borne SAR sensors is becoming an important topic in order to assess whether or not an active landslide may threaten public or private properties and, especially, human life. In this context, the private industry, research institutions, and universities are developing efficient PSI tools for displacement analysis which are increasingly being adapted for its fully operational use.

Despite this advantages, PSI techniques also present some limitations. The displacement information cannot be exploited from all pixels within the illuminate scenario, since mainly due to temporal and spatial decorrelation phenomena [19] only a limited number of pixels, the so-called persistent scatterers, fulfill the phase quality requirements to be included in the PSI processing. This is the case of landslide areas, which typically occur over vegetated regions and, thus, strongly affected by temporal decorrelation phenomena. Two different strategies are mainly employed to detect persistent scatters: these are the coherence stability [6,10], and the Amplitude Dispersion ( $D_A$ ) based technique [3].

In landslide monitoring applications, which generally occur in natural environments, improving the number of high-quality pixels for its later PSI processing results of crucial importance. This fact allows the achievement of more robust networks of persistent scatters and favors the reliable estimation of displacement maps in a major number of points. In this context, different denoising filtering strategies, typically employed in image processing applications to reduce additive Gaussian noise, are being adapted for SAR applications [14, 20–23] demonstrating an excellent performance under multiplicative speckle noise conditions. The rationale is to improve the interferometric phase quality in order to detect the deterministic point-like scatterers, but also the natural distributed scatterers, within the area of interest. This is a key factor in the characterization of landslides, in which improving the density of measurements as far as possible results very useful to achieve a better understanding of landslides' extension and dynamics.

This work presents an advanced PSI processing based on the use of the Nonlocal Interferometric SAR (NL-InSAR) filtering technique presented in [24] for landslide monitoring applications. In this framework, two TerraSAR-X data sets corresponding to the period from April to November 2011, and from August to November 2013, are employed over the landslide area of *El Portalet*, Central Spanish Pyrenees. The DInSAR processing has been addressed employing the Stable Point Network (SPN) technique, which stands for the advanced PSI processing developed by the company Altamira-Information. The objective of this study is to demonstrate the benefits of applying advanced adaptive filtering techniques over natural environments for the retrieval of improved displacement maps. In this context, the results obtained by means of NL-InSAR filtering will be carefully compared in terms of final density and quality with the so-called classical PSI approaches.

Finally, the importance of projecting the displacement results retrieved taking into account the acquisition geometry and the nature of displacement phenomenon is put forward. SAR systems are only sensitive to detect displacements in the line-of-sight (LOS) direction. For this reason, prior to its interpretation or comparison with the ground-truth available, PSI displacement results must be accordingly projected making an assumption about the displacement direction. As it will be shown, with no *a priori* knowledge about the displacement direction, the more realistic model in landslide applications consists on considering that the displacement is produced along the steepest gradient of the terrain slope. DGPS measurements will be showed in this context in order to validate the down-slope hypothesis and hence the final PSI displacement results obtained.

## 2. TEST SITE AND DATA SET

### 2.1 Geological Settings of El Portalet

The test site area selected to evaluate the improvements proposed in this paper corresponds to the landslide of *El Portalet*, located in the upper part of the *Gállego River* basin, in the Central Spanish Pyrenees (*Huesca*). This area and surroundings are characterized by a high density of landslides which have been reactivated due to the constant erosion of the *Gállego River* as well as human activity [25]. In fact, this is the concrete case of the landslides of *El Portalet* area, which were reactivated by the excavation works carried out to build a parking area at the toe of the slope during summer 2004. The area of interest is affected by three main roto-translacional landslides (referred to as A-B-C in Figure 1). The red line in Figure 1 represents the contour of a local slide

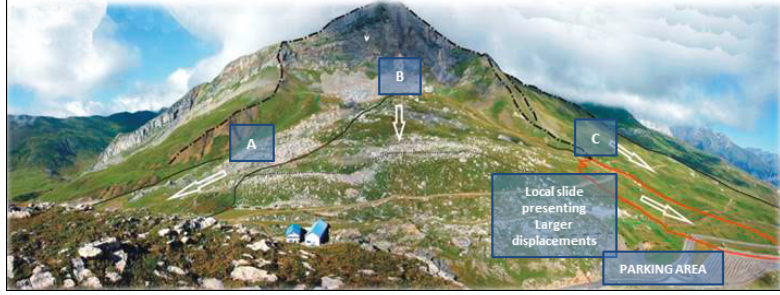


Figure 1. General overview of *El Portalet* landslides.

located over the parking area which is presenting the larger displacements of the area. This local phenomena belongs to the main-lobe of the landslide referred as B in Figure 1.

*El Portalet* landslide area is located on a southwest-facing hillside of *Petasos* Peak, which is 500 m long and 700 m wide and covers 0.35 km<sup>2</sup> in about 12° slope angle [26]. The moving mass also involves intense weathering slates and shales forming high plasticity deposits from the *Devonian* and *Carboniferous* age rocks [27]. This geomechanical features are prone to develop the typical morphologies which characterize unstable slopes, where landslides may occur. Some external features that define typical landslide areas include clearly defined main scarps, hummocky surface topography, high density of surface cracks, streams and pools generated in the landslide limits. The intense rainfalls and the strong topographic gradients intensify the slope mass movement activity in the whole valley.

## 2.2 Previous Works Carried Out over the Area of Interest

As commented above, the excavation works carried out to build the parking located at the foot of the hillside during summer 2004 provoked a local rupture. This fact has motivated an exhaustive monitoring of the area employing several surveying techniques, such as DGPS, extensometers, inclinometers and Ground-Based SAR (GB-SAR), jointly with extensive geological interpretation works, during the last decade.

In this framework, seven total station measurement campaigns were performed from December 2004 to March 2005. Furthermore, several inclinometric readings were carried out between May and October 2005. Before the breakage of the inclinometers installed, the displacement magnitude and extension of an underground rupture surface were detected and measured in the area. Following the stabilization intervention in the slope, five precise DGPS campaigns were carried out in the area from May 2006 to July 2007 indicating a deceleration process in the slope. At this stage, GB-SAR measurements were planned in order monitor the parking landslide while the DGPS campaigns continued. Extra DGPS campaigns carried out until October 2011 completed the whole period of measurements from May 2006 to October 2011 [27].

In order to complete these in-field measurements, several advanced PSI works using space-borne SAR data have been planned to date. A Multi-frequency study with different satellites was performed by the company Altamira-Information using C-band data employing SAR images acquired with ERS and ENVISAT satellites (2001-2007), L-band data from ALOS-PALSAR (2007-2011), and X-band data provided by the TerraSAR-X satellite (2008) [28].

Some modeling works have been also carried out in this area. In this context, a recent study based on a 2D viscoplastic constitutive model [29] has served to validate the extension and the displacement patterns retrieved by means of ground-based and satellite DInSAR techniques.

## 2.3 Data Set

The launch of high-resolution X-band space-borne sensors, such as the German TerraSAR-X satellite or the Italian COSMO-SkyMed constellation, is providing unprecedented amounts of high-resolution data during the last years. This new generation of X-band space-borne sensors reach one order of magnitude better in resolution (up to meter) than its predecessors (ERS-1/2, ENVISAT-ASAR or RADARSAT-1) that used medium resolution with lower bandwidths at C-band, as well as shorter revisit times (from the 11 days in the TerraSAR-X satellite

up to 12 hours for the full COSMO-SkyMed constellation). These new characteristics are offering new exciting opportunities in the frame of landslide monitoring applications. The new generation of X-band space-borne sensors, allow a significant improvement in the monitoring capabilities over man-made structures, such as buildings, bridges, railways and highways, but also over natural stable reflectors, such as rocky areas or bare surfaces. This is strongly related with their high spatial resolution, but also with the shorter revisit time, thus improving the temporal and spatial sampling for geo-hazard assessment applications.

To continue with the monitoring of *El Portalet* carried out during the last years, two TerraSAR-X data sets acquired in ascending mode, with the objective to maximize the sensor sensitivity to the displacement (as it will be explained in Section 5), have been selected. The fast temporal decorrelation phenomenon present at X-band over this type of natural environments represents hence a perfect test site to demonstrate the benefits of using NL-InSAR for PSI purposes. The first data set is composed by 13 TerraSAR-X images acquired during the period corresponding from April 2011 to November 2011. The second one is composed by 8 TerraSAR-X images acquired during the period corresponding from August to November 2013.

In order to improve the PSI performance 7 Artificial Corner Reflectors (ACR) for radar satellite were installed in September 2010. In 2013, an intensification of the ACR network, adding 11 new ACRs, was carried out in the main slope of *El Protalet*. Finally an Automatic Inclinometer System (AIS) [30–32] was installed in a new borehole in August 2013. DGPS over the new ACRs installed and over other interesting points of the landslide have been collected to date.

### 3. METHODOLOGY FOR MEASURING TERRAIN DISPLACEMENTS

#### 3.1 Differential SAR Interferometry

DInSAR techniques are based on exploiting the phase-difference, i.e, the interferogram  $\varphi_{int}$  from a pair of SAR images, and analyze the different contribution terms of the resulting wrapped differential phase terms. The interferogram phase is characterized by varying between the range of  $[-\pi, \pi]$ , and it is typically formulated in relative terms as the increment between two different pixels of the interferogram as follows [19]

$$\Delta\varphi_{int} = \Delta\varphi_{flat} + \Delta\varphi_{topo} + \Delta\varphi_{displ} + \Delta\varphi_{APS} + \Delta\varphi_{noise} = \frac{4\pi}{\lambda R_0} \cdot \frac{B_n}{\tan(\theta_{inc})} \cdot \Delta r + \frac{4\pi}{R_0} \cdot \frac{B_n}{\sin(\theta_{inc})} \cdot \Delta h + \frac{4\pi}{\lambda} \cdot \Delta\rho + \Delta\varphi_{APS} + \delta\varphi_{noise} \quad (1)$$

where  $\theta_{inc}$  refers to the incidence angle,  $B_n$  indicate the perpendicular baseline,  $\Delta r$  and  $\Delta h$  accounts for the range distance and height difference, respectively,  $R_0$  refers to the absolute range distance in the LOS direction between the sensor and the target, and  $\lambda$  accounts for the wavelength.  $\Delta\varphi_{flat}$  and  $\Delta\varphi_{topo}$  are referred to as the flat-earth and the topographic components. These phase contributions are affected by variations of the relative range distance between the sensor and the target during the different acquisitions.  $\Delta\varphi_{flat}$  accounts for the situation of illuminating a flat surface, while  $\Delta\varphi_{topo}$  is related with the existing topography in the illuminated area.  $\Delta\varphi_{displ}$  is the phase term of interest since it is related with the ground displacement undergone  $\Delta\rho$  in the LOS direction along the different SAR acquisitions.  $\Delta\varphi_{APS}$  accounts for the phase disturbances produced due to the changing atmospheric conditions. Finally, the phase term referred as  $\Delta\varphi_{noise}$  include the phase degradation artifacts produced by the scatters' changes along the temporal axis (temporal decorrelation), the slightly variations of the incident angle between the different acquisitions (spatial decorrelation), and the thermal noise inherent to the SAR system.

The objective of DInSAR techniques is to isolate the displacement component  $\Delta\rho$ . For this purpose, the phase contribution related with topography  $\Delta\varphi_{topo}$  is typically compensated making use of the orbital information and an external Digital Elevation Model (DEM) of the illuminated area. Once this phase term is estimated, the so-called differential interferograms are obtained. Since DEMs normally have some inaccuracies, it is impossible to completely compensate the topographic phase contribution. This fact leads to a new term related to the DEM inaccuracies  $\Delta\varepsilon_{DEM}$ , which will be referred to as topographic error in the following. Taking in to account all these considerations the final differential phase  $\Delta\varphi_{dif}$  is expressed as follows

$$\Delta\varphi_{dif} = \Delta\varphi_{\varepsilon_{DEM}} + \Delta\varphi_{displ} + \Delta\varphi_{APS} + \Delta\varphi_{noise} = \frac{4\pi}{\lambda R_0} \cdot \frac{B_n}{\sin(\theta_{inc})} \cdot \Delta\varepsilon_{DEM} + \frac{4\pi}{\lambda} \cdot \Delta\rho + \Delta\varphi_{APS} + \Delta\varphi_{noise} \quad (2)$$

### 3.2 The SPN Technique

PSI is an evolution of DInSAR techniques that makes use of a multi-temporal stack of differential interferograms in order to overcome the limitations of classical DInSAR, i.e., the presence of atmospheric artifacts, the remaining topographic errors due to inaccuracies in the DEM employed during the generation of differential interferograms but, above all, the negative impact of temporal and spatial decorrelation phenomena. PSI allows the retrieval of the linear and non-linear components of displacement, the topographic error and the APS.

Several advanced PSI processing chains have been developed in the last decade to estimate surface displacements with extremely high accuracy [2–5, 7–15]. The work presented in this paper has been carried out using the SPN, which stands for the advanced PSI technique developed by the company Altamira-Information since 2002 [8].

In order to perform precise estimations, only those pixels that are not affected by decorrelation are first detected. The reliability of any PSI processing technique is compromised by the phase quality of the differential interferograms available. Mainly due to temporal decorrelation phenomena, only a limited number of them fulfill the phase quality requirements to achieve reliable displacement map estimations. For this reason, prior to the application of any PSI technique, an adequate selection of reliable high-quality pixel candidates is mandatory, i.e., the so-called persistent scatterers. The point density depends on the land cover (urban, vegetated, arid, etc.), but values of several thousands of measurement pixels per square kilometer are typically obtained. As it will be showed in the following Section, the number of high-quality pixels for the SPN processing can be improved applying advanced adaptive filtering techniques.

Regarding the interferogram selection for the SPN processing, notice that the displacement term depends on the temporal distribution, and not on the spatial baseline distribution. Contrarily, the topographic error term is sensible to the spatial baseline, but not to the temporal distribution of data. Following this argument, it is interesting to have a data set collection with a good temporal sampling, i.e. without large temporal gaps and uniformly distributed, and with the less possible spatial baselines between interferometric pairs. Despite this, the SPN is able of producing reliable products even in conditions of large spatial baselines, closer to the critical baseline, or platform instabilities.

As seen in Eq. (2) (in Section 3.1) the evolution of the differential interferometric phase along the temporal stack is directly related to the ground displacement produced, but there are other artifacts that may compromise the reliability of the displacement estimation process. On the one hand, as seen above, the real height of the stable points considered for the PSI processing can differ from what it is indicated by the DEM depending on its accuracy. This height error has a negative impact for PSI purposes and must be accordingly estimated. On the other hand, the impact of the APS must be also considered. The variability of the atmospheric artifacts during data set also affect the differential phase. Due to the atmospheric changing conditions, the delay that occurs when an electromagnetic wave passes through the different layers of the atmosphere is variable from one image to another, but also within the same image depending on the location. These effects must be estimated and compensated for in order to obtain a precise measurement of the actual displacement. The common approach to compensate APS consists on taking advantage of their particular temporal and spatial frequency behavior. This problem is typically addressed through a low pass filtering process [19] which also allows to cancel the different offsets between the differential interferograms available.

The SPN consists on a pixel-by-pixel process to obtain the linear and non-linear components of displacement, but also the topographic error and the APS. The first block of the SPN is based on adjusting a linear model-based solution to the differential interferograms available, taking into account the different terms of the differential phase equation seen in Eq. (2). This estimation is performed pixel-by-pixel without the employment of any spatial interpolation. As a result, a reliable mean annual deformation rate and a topographic DEM error is obtained for the persistent scatterers available. At this stage, the so-called model coherence is defined in order to measure the quality of the solutions. The model coherence ranges in the interval [0, 1], reaching high values when the linear model perfectly fits the data. Otherwise, it tends towards zero when the model adjustment is poor. With this function it is possible to discard noisy pixels due to a bad adjustment.

Once the linear estimation step is finished, the SPN is able to provide time series related with the temporal evolution of the total displacement. For this purpose, the linear model estimated previously and the APS are

removed from the original differential interferograms leading to the so-called phase residues, which will only contain the non-linear component of displacement. The rationale is to re-order these differential residues along the temporal axis to obtain the absolute non-linear displacement per image to subsequently add them to the linear model estimated in the previous step. Time series are typically employed to identify non-linear patterns and identify possible accelerations. The accuracy of the process is roughly 2-5 mm. This value depends on the satellite, the number of images and of the quality of the measurement points. Time series can be optionally filtered in order to reduce the possible remaining noise and ease the interpretation of the final results.

## 4. PSI PROCESSING BASED ON NL-INSAR FILTERING

### 4.1 Classical Persistent Scatters Selection Methods

Two main criteria are available in the literature for the estimation of the pixels' phase quality. These are the coherence stability [6,10] and the amplitude dispersion [3]. Both methods stand for the selection of the persistent scatters available in the area of interest, which will be characterized by exhibiting high-quality phase values along the whole temporal data set.

In the former approach, the phase quality of each pixel is achieved through the calculation of the interferometric coherence [19]

$$\gamma = |\gamma| e^{j\varphi} = \frac{E \{S_1 \cdot S_2^*\}}{\sqrt{E \{|S_1|^2\} \cdot E \{|S_2|^2\}}} \quad (3)$$

where  $S_1$  and  $S_2$  refer to the complex values corresponding to the same pixel of the two SAR acquisitions forming the interferogram,  $|\cdot|$  accounts for the absolute value operator, and  $E \{\cdot\}$  indicate the expectation value operator. There is a direct relationship between the coherence values and the interferometric phase dispersion, as demonstrated in [19,33]. Coherence values range between [0, 1], attending these two limit situations for the cases of totally uncorrelated and correlated data, respectively.

In practice, under the assumption of ergodicity and considering locally stationary processes, the expectation operator  $E \{\cdot\}$  may be replaced by a spatial averaging around the pixel of study leading the maximum likelihood estimator of the coherence [33], which can be expressed for each spatial pixel  $(m, n)$  as follows

$$|\hat{\gamma}(m, n)| = \frac{\left| \sum_{i=0}^{L_1-1} \sum_{j=0}^{L_2-1} S_1(m, n) \cdot S_2^*(m, n) \right|}{\sqrt{\left( \sum_{i=0}^{L_1-1} \sum_{j=0}^{L_2-1} |S_1(m, n)|^2 \right) \left( \sum_{i=0}^{L_1-1} \sum_{j=0}^{L_2-1} |S_2(m, n)|^2 \right)}} \quad (4)$$

where  $L_1$  and  $L_2$  refer to the window size in the range and azimuth dimensions respectively, and  $N = L_1 \times L_2$  indicates the multi-look carried out, which accounts for the number of pixels involved in the spatial averaging.

To obtain temporal sensitivity along the whole stack of  $N_{\text{int}}$  differential interferograms, the mean coherence map  $\hat{\gamma}_t$  is typically computed through a temporal average of the single interferometric coherence maps as follows

$$|\hat{\gamma}_t| = \frac{2}{N(N-1)} \sum_{i=1}^{N_{\text{int}}} |\hat{\gamma}| \quad (5)$$

At this stage a threshold of mean coherence is fixed and only those pixels exhibiting coherence values above the threshold established are selected as reliable for the displacement map estimation. Due to the multi-looking process carried out, this approach is more suited for selecting distributed scatterers in natural environments, but it also allows the detection of point-like deterministic ones, especially when working with small multi-look values at high frequencies, such as X- or Ku-bands.

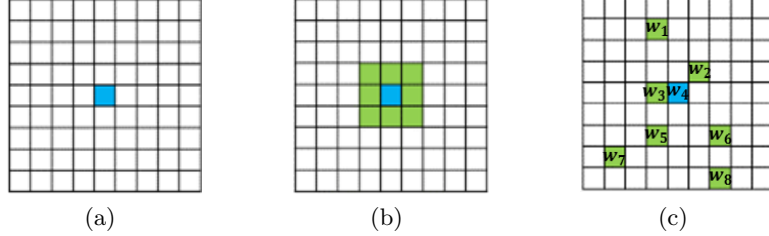


Figure 2. Comparison between (a) full-resolution, (b) boxcar, and (c) adaptive NL-InSAR filtering.

In the later approach, the phase dispersion of targets within the illuminated scenario is established through the  $D_A$  index [3] as follows

$$D_A = \frac{\sigma_A}{m_A} \quad (6)$$

where  $m_A$  and  $\sigma_A$  refer to as the mean and the standard deviation of the amplitude temporal evolution, respectively.

Under this approach, the phase dispersion is proportional to the  $D_A$  index in those pixels with high values of signal-to-noise ratio (SNR). This technique seeks the detection of the so-called Permanent Scatterer (PS), which are targets that behave as deterministic point-like scatterers for the whole temporal stack of SAR images in terms of its amplitude behavior. PSs are theoretically not affected by decorrelation artifacts. In practice, those targets characterized by having lower values of  $D_A$ , typically less than 0.25, are selected as reliable for the PSI processing [3].

The SPN is able to work with the coherence stability or the amplitude dispersion approaches working with either multi-looked or full-resolution interferograms, respectively. In this framework, the choice of the pixel selection approach depends on the nature of the high-quality targets in the illuminated area. The coherence stability pixel selection method requires performing a multi-look of the interferograms, which allows reducing the speckle noise, but also yields to a loose of the spatial resolution. Contrarily, the  $D_A$  pixel selection approach preserve the full-resolution of the SAR images.

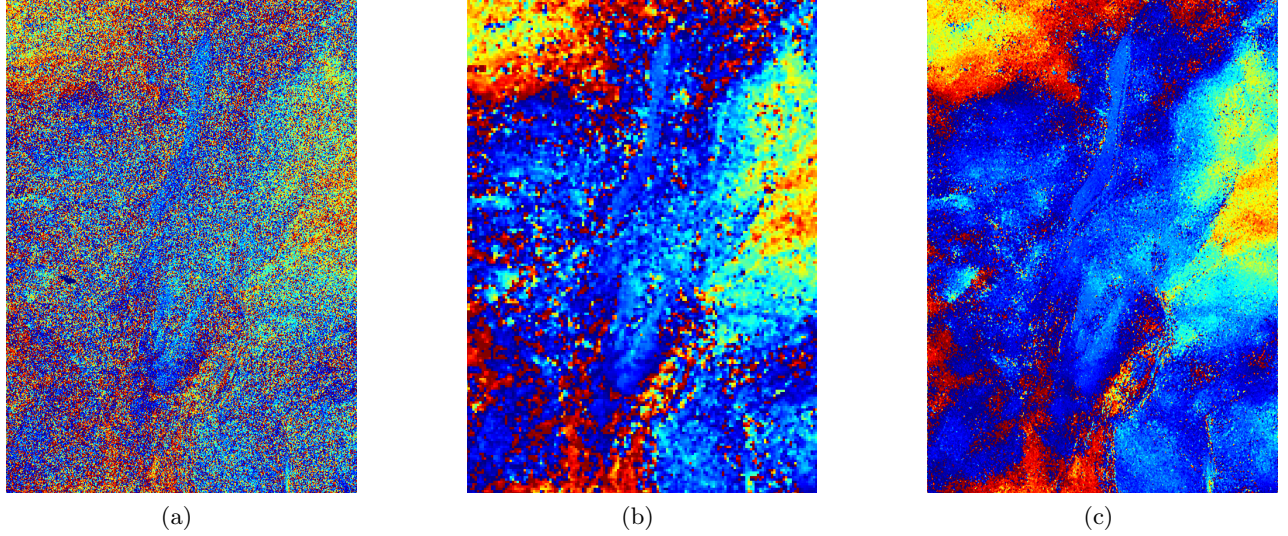
There is hence a clear limitation when working in natural environments characterized by containing different types of land covers with presence of both, point-like and distributed scatterers. Exploring the major number of points results of crucial importance in these type of scenarios. In this context, different denoising filtering strategies, typically employed in image processing, are recently being adapted for SAR applications [14, 20–23].

The following Section presents the application of the adaptive NL-InSAR filtering technique presented in [24] for the retrieval of reliable densified displacements maps by means of PSI. This advanced PSI processing allows the joint detection and exploitation of point-like and distributed scatterers preserving the original resolution of SAR images and largely improving the displacement retrieval process.

## 4.2 NL-InSAR

NL-InSAR filtering consists on a probabilistic criterion based on both the intensities and the interferometric phases that surround two given patches. Nonlocal filter uses the concept of local redundancy for estimating, pixel-by-pixel, the scene components preserving the resolution of the image. This methodology allows us to consider pixels that are far apart rather than restricting the similar pixels that belong to a local neighborhood, such as boxcar filtering (see Figure 2).

One pixel is assumed to come from the same statistical population as the given pixel if the patches that surround both pixels present a high similarity measure. The filtered pixel is obtained by a weighted combination of pixel values which can be far apart inside the search window (see Figure 2(c)). The weights are computed by using the maximum likelihood estimator (WMLE) and are iteratively refined by comparing patches of previous estimates and patches of the noisy image [24].

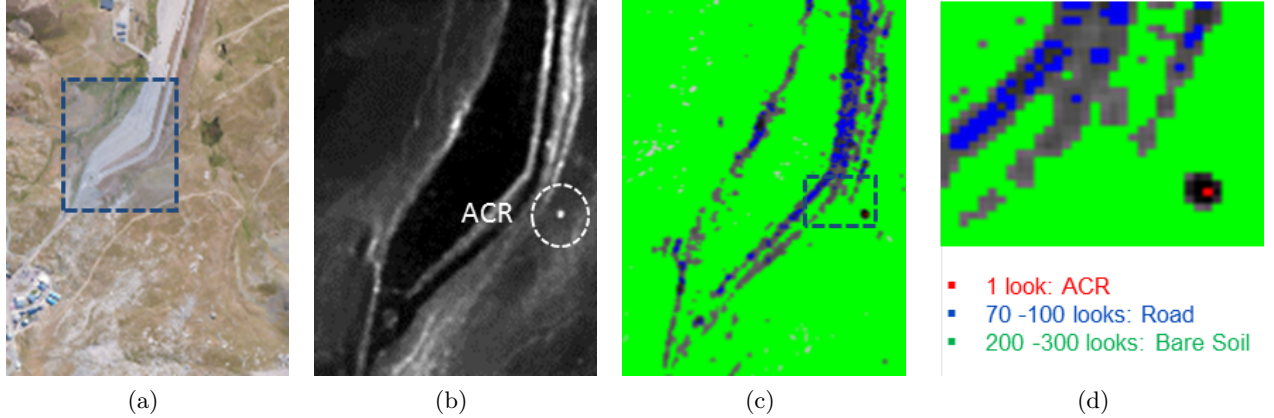


(a)

(b)

(c)

Figure 3. (a) Full-resolution interferogram. Filtered interferogram after applying (b) a  $5 \times 5$  boxcar window and (c) adaptive NL-InSAR filtering.



(a)

(b)

(c)

(d)

Figure 4. Different number of looks obtained in 3 different land covers. (a) Optical image corresponding to the parking area of *El Portalet*. (a) SAR Reflectivity image of the area indicated with a blue square in (a). The white circle indicates the location of an ACR. (c) Different number of looks obtained over the bare soil, the road and the ACR available within the selected area. (d) Zoom of the area indicated with a blue square in (c).

Figure 3 illustrate the benefits of applying NL-InSAR filtering to improve the quality of the available differential interferograms. Figure 3(a) show the original interferogram at full-resolution, while Figure 3(b)-(c) show the resulting differential interferogram after applying a  $5 \times 5$  boxcar window and a NL-InSAR filtering using a patch window of 5 pixels and a search window of 20 pixels. Notice the goodness of NL-InSAR filtering which smooths the noise over the homogeneous regions while maintains the resolution over the deterministic point-like scatterers.

Under this approach the number of looks varies from one pixel to another as it depends on the number of similar patches found in the search window around the pixel under analysis. The sizes of the patch window and the search window were set as a trade-off between having one look in the ACRs present in the scene, thus ensuring enough noise reduction over the homogeneous areas. This fact is illustrated in Figure 4 which shows the different number of looks obtained in 3 different land covers. Notice how the number of looks is larger over the bare surfaces of the area studied, while the ACR has only 1 look, as it should be, since it is a deterministic

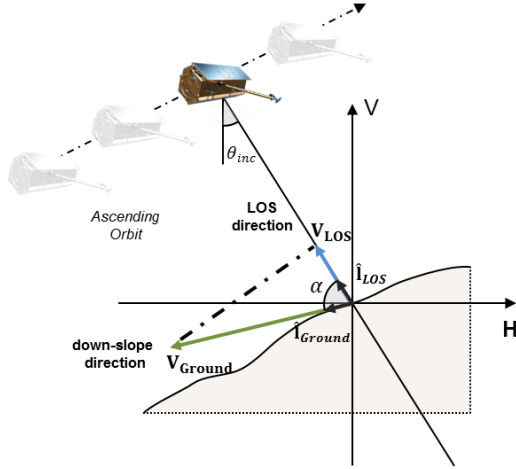


Figure 5. Geometry of acquisition under down-slope displacement assumption.

point-like scatterer.

Once the interferograms are filtered, the PSI processing is totally equivalent, being no difference with respect to the classical approaches.

## 5. DOWN-SLOPE PROJECTION OF LOS DISPLACEMENT VECTORS

SAR systems only have sensitivity in the LOS direction, therefore, the displacement maps obtained by means of PSI techniques are always relative to the slant-range plane. For the current polar-orbiting SAR space-borne sensors, the look direction is either east or west, for ascending or descending orbits, respectively. For this reason, SAR sensors only are able to detect movements along slopes facing either east or west, and almost insensitive to movements in north or south directions. This aspect should be taken into account when planning the SAR acquisitions. In the context of landslide applications, the more realistic assumption regarding the displacement direction is based on considering that it is produced along the steepest gradient of the slope. Computing the percentage of measured displacement in the LOS direction is mandatory to ensure the reliability of the results. For the study case presented in this paper the ascending mode resulted more suited since the projection factor between the displacement and LOS directions was lower compared with the one provided by the descending mode. The ascending mode was hence finally selected in order to maximize the percentage of displacement detected by the space-borne sensor.

Another factor to take into account in these kind of applications is related with the interpretation of PSI results. Over flat areas this fact does not represent any difficulty since the displacements are typically addressed as negative departing from the sensor (for subsidence phenomena) and positive approaching the radar (for uplift phenomena). On the contrary, when facing areas with steep topography, as in the present case, the interpretation of the final results becomes more complex. If the slope of the mountain is facing the satellite, any land movement along the down-slope direction will be towards the satellite. Contrarily, the same displacement will be detected as moving away from the SAR sensor if the slope is opposite.

Finally, due to this particular acquisition geometry, some geometrical distortions should be also taken into account when planning the acquisitions and, furthermore, in the final interpretation of the displacement results. Three main geometrical distortions are present in the SAR images: the foreshortening, the layover and the shadowing [19]. The foreshortening effect is visible when those slopes facing to the radar are compressed when projected onto the slant-range image plane. As the local slope angle is closer to the incidence angle the effect is more pronounced. The extreme case appears when both angles are equal; in this case the slope is represented by a single point in the image showing very high reflectivity values. Points affected by strong foreshortening

will not have reliable information and should be filtered out. The layover distortion occurs when the angle of a slope facing to the radar exceeds the angle of incidence. Due to this inverse effect in the echo arrival order, higher points are closer to the radar appearing earlier in the SAR image. From an intuitive point of view, the tops of the mountains appear before than the valleys. These points are not of practical utility and should be also removed from the processing. Finally, the shadowing effect occurs when a slope opposite to the radar has a steeper slope than the incidence angle. This causes some parts to be not illuminated by the SAR sensor, the so-called shaded areas, and thus, no reflectivity or phase information from these area will be collected.

Under the argument described above, the measured displacements in the LOS direction are rarely the real ones, but a projection of them. Following a vector notation, both velocities may be expressed mathematically as follows

$$\begin{aligned}\mathbf{V}_{LOS} &= |\mathbf{V}_{LOS}| \cdot \hat{\mathbf{l}}_{LOS} \\ \mathbf{V}_{Ground} &= |\mathbf{V}_{Ground}| \cdot \hat{\mathbf{l}}_{Ground}\end{aligned}\tag{7}$$

where  $\mathbf{V}_{Ground}$  accounts the ground velocity vector, i.e., the real ground displacement, and  $\mathbf{V}_{LOS}$  the measured velocity vector, which is a projection of the previous one in the LOS direction. The magnitudes  $|\mathbf{V}_{LOS}|$  and  $|\mathbf{V}_{Ground}|$  account for the magnitude of the displacements, and the unitary vectors  $\hat{\mathbf{l}}_{LOS}$  and  $\hat{\mathbf{l}}_{Ground}$  are related with the displacement directions. Since the former is a projection of the latter the intensity of both vectors may be related through a scalar product as indicated in the following

$$|\mathbf{V}_{LOS}| = |\mathbf{V}_{Ground}| \cdot \cos(\alpha)\tag{8}$$

where

$$\cos(\alpha) = \hat{\mathbf{l}}_{LOS} \cdot \hat{\mathbf{l}}_{Ground},\tag{9}$$

being  $\alpha$  the angle formed by both unitary vectors.

When the ground displacements produced over the affected area are expected to be in the vertical direction over flat areas, as typically occur with subsidence or uplift phenomena in urban scenarios,  $\alpha$  directly becomes the incidence angle  $\theta_{inc}$ . Contrarily, in landslide monitoring applications the problem becomes more complex since the real ground displacement of each spatial point has a topographic dependence related with the local slope in each position. As seen above, the more realistic assumption of the displacement direction with no *a priori* knowledge consists on considering that the displacement is produced along the steepest gradient of the terrain slope. This information may be directly derived employing an accurate DEM of the illuminated area, and the angle  $\alpha$  may hence be obtained through Eq. (9). Figure 5 shows the geometry of acquisition under the down-slope displacement assumption described in this Section.

Once the displacement vectors are accordingly projected they can be geocoded in map coordinates and be visualized by using a virtual globe viewer or a Geographical Information System (GIS) software.

## 6. RESULTS AND DISCUSSION

This Section presents the final accumulated displacement maps over the area of *El Portalet* by means of the NL-InSAR filtering technique presented in Section 4. Furthermore, the importance of projecting down-slope the final PSI results, as stated in Section 5, is put forward.

Figure 6 shows a comparison of accumulated displacements in the LOS corresponding to the 2013 TerraSAR-X data set using the full-resolution  $D_A$  approach (see Figure 6(a)), the coherence stability approach using a  $5 \times 5$  boxcar window (see Figure 6(b)), and after applying the NL-InSAR filtering technique proposed in Section 4 (see Figure 6(c)). To ensure a fair comparison, equivalent thresholds over the three methodologies have been established in order to provide the same requirements in terms of phase standard deviation. As expected, all approaches are retrieving almost identical displacement trends except for the increase in pixels' density. Figure 7

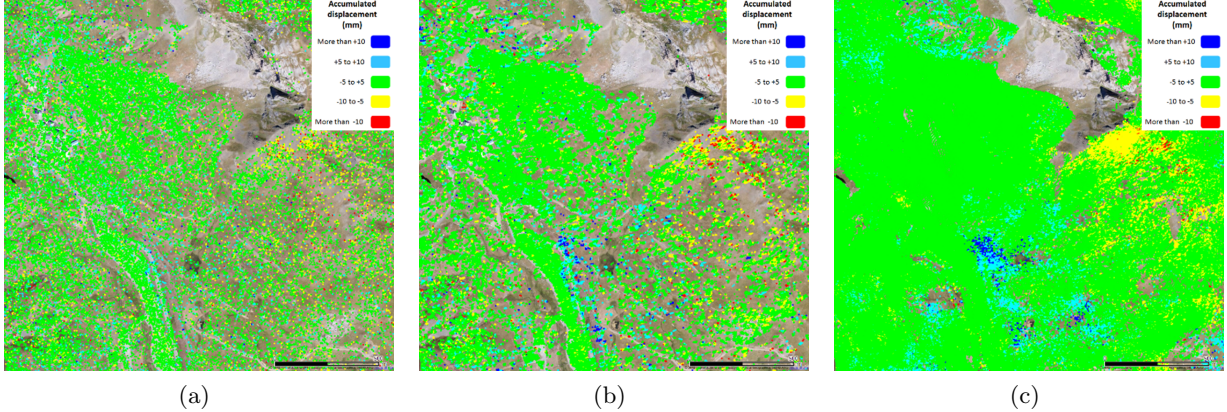


Figure 6. PSI Displacement results in the LOS direction using a (a) full-resolution PSI processing, after applying a (b)  $5 \times 5$  boxcar window, and after applying (c) NL-InSAR filtering technique. This results correspond to the 2013 data set described in Section 2.

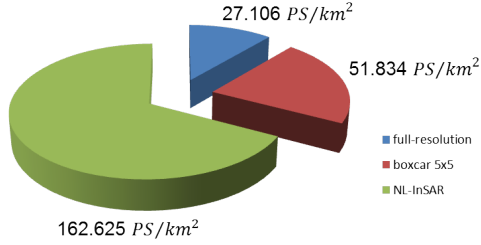


Figure 7. Pixels' density in  $PS/km^2$  for the full-resolution PSI, and after applying a  $5 \times 5$  boxcar window and NL-InSAR filtering approaches.

gives a quantitative information of the number of pixels selected. As expected, PSI results based on NL-InSAR filtering show an outstanding improvement (roughly a threefold increase) in the detection of natural targets (bare soil, roads, rocks) compared with classical PSI approaches. As seen in Section 4, this advanced adaptive filtering technique allows the joint detection and exploration of point-like and distributed scatterers, thus benefiting the PSI processing. It must be pointed out that the availability of ACR in the area of interest, presented in Section 2, have allowed the maximization of the filter response.

The increase in terms of pixel's density showed by the NL-InSAR approach represents key factor in the characterization of the landslides available in the area of study. This enhancement allows increasing the density of measurements allowing an improvement in determining landslides' extension and dynamics.

As stated in Section 5, prior to the interpretation of the displacements results retrieved, PSI products should be projected assuming a down-slope displacement model. Figure 8 shows the final accumulated down-slope displacement results over the area of *El Portalet* from the two TerraSAR-X data sets available.

The final down-slope accumulated displacement maps obtained reveal that several slope instabilities occur in *El Portalet* area (see Figure 8). Notice that the results corresponding to both periods are in concordance since they show similar displacement patterns. As expected, some instabilities may be noticed in the A, B, and C landslide areas described in Figure 1. Main displacement points up to 30 cm (from April to November 2011) and up to 10 cm (from August to November 2013) may be identified at the toe of landslide B (see Figure 8). This region corresponds to the local slide which is occurring over the parking area. As commented in Section 2, this region is exhibiting the larger displacements of the area during the last years (red contour area represented in Figure 1). As expected, local and distributed displacement patterns are also appreciated in landslides areas A and C for both periods. These are clearly identified after applying the down-slope projection factor.

These conclusions are coherent with the previous results obtained through the in-field campaigns and DInSAR results presented in [27–29]. In addition, the displacement maps obtained during 2011 show a high agreement with

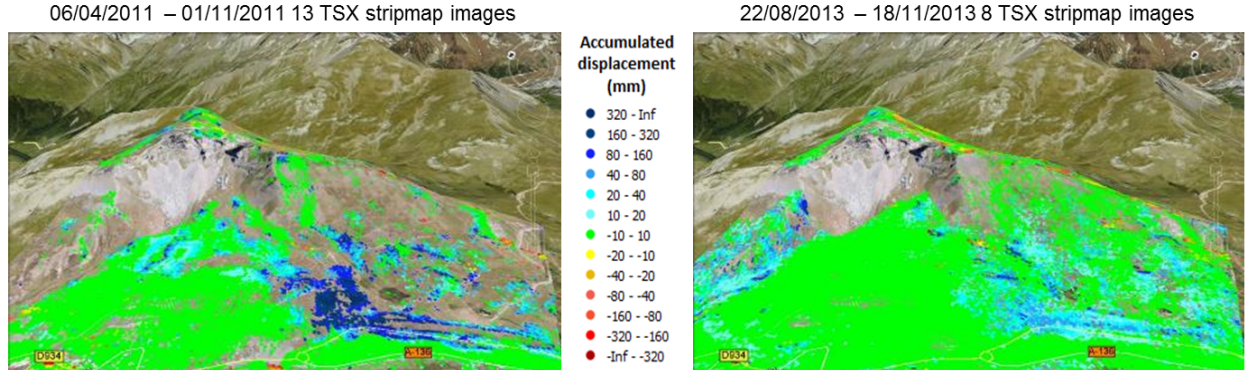
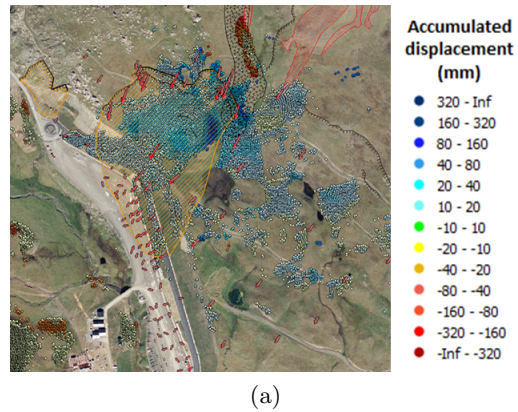


Figure 8. NL-InSAR down-slope accumulated displacement results over the area of *El Portalet* from the 2011 and 2013 TerraSAR-X data sets presented in Section 2.



(a)

Figure 9. Comparison between the down-slope accumulated PSI results (points) presented in Figure 8 and the displacements vectors retrieved through the DGPS campaigns carried out during 2011 (red arrows) in the parking area.

the conclusions extracted from the DGPS campaigns presented in Section 2, as illustrated in Figure 9. This figure shows a comparison between the down-slope PSI results (points) presented in Figure 8 and the displacements vectors retrieved through the DGPS campaigns carried out during 2011 (red arrows) in the parking area. A good correlation in terms of spatial extension and magnitudes may be appreciated, thus validating the down-slope displacement assumption proposed in the paper. Furthermore, notice how the location of main scarps of the landslide area, defined by geomorphological interpretation (black line and orange polygon in Figure 9), are in agreement with the PSI displacements detected.

## 7. CONCLUSIONS

In this paper advanced PSI improvements to enhance the displacement retrieval process over natural environments with different land covers have been presented. The work has been carried out using the SPN, which stands for the advanced PSI technique developed by the company Altamira-Information.

The test site selected to evaluate the methodology proposed correspond to the well-known mountainous environment of *El Portalet*, Central Spanish Pyrenees. This area is characterized by a high density of landslides which were reactivated by the excavation works carried out to build a parking area during summer 2004. In this

framework, two TerraSAR-X data sets corresponding to the period from April to November 2011 and from August to November 2013, respectively, have been studied. In fact, an exhaustive monitoring of this area employing several surveying techniques, such as DGPS, extensometers, inclinometers and GB-SAR, jointly with precise geological interpretation works, has been carried out during the last decade.

The employment of the NL-InSAR filtering technique presented in [24] has been proposed in order to enhance the number of reliable high-quality pixels and its quality during the PSI processing. The objective has been to improve the interferometric phase quality to detect both the deterministic point-like scatterers and the natural distributed scatterers available in the area of interest maintaining the full-resolution of the original SAR images. In this framework, a comparison with the so-called classical approaches has been proposed. PSI results presented have demonstrated to improve the density and quality of displacement estimations. As seen, this is a key factor in landslide monitoring applications which normally occur in natural environments largely affected by temporal decorrelation phenomena which are typically characterized by a poor number of persistent scatterers detected.

Prior to the results interpretation, it has been proposed the application of a down-slope displacement model. Since SAR systems only have sensitivity in the LOS direction, the down-slope projection of the measured displacement vector has been demonstrated to be mandatory in order to achieve a correct understanding of the displacements retrieved.

The final displacement results obtained, corresponding to both TerraSAR-X data sets, present similar displacement patterns, showing a high agreement with the previous field and PSI results presented over the area of interest. Finally, DGPS measurements coinciding with the data set corresponding to 2011, have been presented in order to validate the down-slope hypothesis, and thus the final PSI displacement results obtained. Some future work lines may include the validation of the data set corresponding to 2013 with the DGPS and the AIS measurements carried out during this year.

## ACKNOWLEDGMENTS

This research work has been funded by the European Union Seventh Framework Programme (FP7/2007-2013) in the framework of the LAMPRE project (Grant Agreement 312384).

The authors would like to thank Dr. Gerardo Herrera, Dr. Juan Carlos García Dávalillo and Dr. José Antonio Fernández Merodo from the Geohazards InSAR Laboratory and Modelling Group of the Instituto Gelógico y Minero de España, Madrid (España), and Dr. Paolo Allasia, Dr. Piernicola Lollino and Dr. Andrea Manconi from the Istituto di Ricerca per la Protezione Idrogeologica, Consiglio Nazionale delle Ricerche, Torino (Italy) for the field instrumentation campaigns carried out and for their helpful discussions and support in the interpretation of the final displacement results obtained.

## REFERENCES

- [1] Massonnet, D. and Feigl, K. L., "Radar interferometry and its application to changes in the Earth's surface," *Reviews of Geophysics* **36**(4), 441 (1998).
- [2] Ferretti, A., Prati, C., and Rocca, F., "Nonlinear subsidence rate estimation using permanent scatterers in differential SAR interferometry," *IEEE Transactions on Geoscience and Remote Sensing* **38**(5), 2202–2212 (2000).
- [3] Ferretti, A., Prati, C., and Rocca, F., "Permanent Scatterers in SAR interferometry," *IEEE Transactions on Geoscience and Remote Sensing* **39**(1), 8–20 (2001).
- [4] Mora, O., Mallorqui, J. J., and Duro, J., "Generation of deformation maps at low resolution using differential interferometric SAR data," in [*IEEE International Geoscience and Remote Sensing Symposium*], **5**(C), 2696–2698, IEEE (2002).
- [5] Berardino, P., Fornaro, G., Lanari, R., and Sansosti, E., "A new algorithm for surface deformation monitoring based on small baseline differential SAR interferograms," *IEEE Transactions on Geoscience and Remote Sensing* **40**, 2375–2383 (Nov. 2002).
- [6] Mora, O., Mallorqui, J., and Broquetas, A., "Linear and nonlinear terrain deformation maps from a reduced set of interferometric sar images," *IEEE Transactions on Geoscience and Remote Sensing* **41**, 2243–2253 (Oct. 2003).

- [7] Werner, C., Wegmüller, U., Strozzi, T., and Wiesmann, A., "Interferometric point target analysis for deformation mapping," in [*IGARSS 2003. 2003 IEEE International Geoscience and Remote Sensing Symposium. Proceedings (IEEE Cat. No.03CH37477)*], **7**(1), 4362–4364, IEEE (2003).
- [8] Arnaud, A., Adam, N., Hanssen, R., Inglada, J., Duro, J., Closa, J., and Eineder, M., "ASAR ERS interferometric phase continuity," in [*IGARSS 2003. 2003 IEEE International Geoscience and Remote Sensing Symposium. Proceedings (IEEE Cat. No.03CH37477)*], **2**(C), 1133–1135, IEEE (2003).
- [9] Hooper, A., "A new method for measuring deformation on volcanoes and other natural terrains using InSAR persistent scatterers," *Geophysical Research Letters* **31**(23), L23611 (2004).
- [10] Lanari, R., Mora, O., Manunta, M., Mallorqui, J. J., Berardino, P., and Sansosti, E., "A small-baseline approach for investigating deformations on full-resolution differential SAR interferograms," *IEEE Transactions on Geoscience and Remote Sensing* **42**, 1377–1386 (July 2004).
- [11] Blanco-Sánchez, P., Mallorquí, J. J., Duque, S., and Monells, D., "The Coherent Pixels Technique (CPT): An Advanced DInSAR Technique for Nonlinear Deformation Monitoring," *Pure and Applied Geophysics* **165**, 1167–1193 (Aug. 2008).
- [12] Hooper, A., "A multi-temporal InSAR method incorporating both persistent scatterer and small baseline approaches," *Geophysical Research Letters* **35**, L16302 (Aug. 2008).
- [13] Fornaro, G., Reale, D., and Serafino, F., "Four-Dimensional SAR Imaging for Height Estimation and Monitoring of Single and Double Scatterers," *IEEE Transactions on Geoscience and Remote Sensing* **47**, 224–237 (Jan. 2009).
- [14] Ferretti, A., Fumagalli, A., Novali, F., Prati, C., Rocca, F., and Rucci, A., "A New Algorithm for Processing Interferometric Data-Stacks: SqueeSAR," *IEEE Transactions on Geoscience and Remote Sensing* **49**, 3460–3470 (Sept. 2011).
- [15] Iglesias, R., Mallorqui, J. J., and Lopez-Dekker, P., "DInSAR Pixel Selection Based on Sublook Spectral Correlation Along Time," *IEEE Transactions on Geoscience and Remote Sensing* **52**, 3788–3799 (July 2014).
- [16] Kwok, R. and Fahnestock, M., "Ice sheet motion and topography from radar interferometry," *IEEE Transactions on Geoscience and Remote Sensing* **34**(1), 189–200 (1996).
- [17] Refice, A., Bovenga, F., Guerriero, L., and Wasowski, J., "DInSAR applications to landslide studies," in [*IGARSS 2001. Scanning the Present and Resolving the Future. Proceedings. IEEE 2001 International Geoscience and Remote Sensing Symposium (Cat. No.01CH37217)*], **1**(2), 144–146, IEEE (2001).
- [18] Kim, S.-w., Member, S. S., and Won, J.-s., "Measurements of soil compaction rate by using JERS-1 SAR and a prediction model," *IEEE Transactions on Geoscience and Remote Sensing* **41**, 2683–2686 (Nov. 2003).
- [19] Hanssen, R., [Radar interferometry: data interpretation and error analysis], kluwer aca ed. (2001).
- [20] Deledalle, C.-A., Denis, L., and Tupin, F., "Iterative weighted maximum likelihood denoising with probabilistic patch-based weights," *IEEE transactions on image processing : a publication of the IEEE Signal Processing Society* **18**, 2661–72 (Dec. 2009).
- [21] Deledalle, C.-A., Tupin, F., and Denis, L., "Polarimetric SAR estimation based on non-local means," in [*2010 IEEE International Geoscience and Remote Sensing Symposium*], 2515–2518, IEEE (July 2010).
- [22] Alonso-gonzález, A., López-martínez, C., Member, S., and Salembier, P., "Filtering and Segmentation of Polarimetric SAR Data Based on Binary Partition Trees," *IEEE Transactions on Geoscience and Remote Sensing* **50**(2), 593–605 (2012).
- [23] Alonso-González, A., López-Martínez, C., Salembier, P., and Deng, X., "Bilateral Distance Based Filtering for Polarimetric SAR Data," *Remote Sensing* **5**, 5620–5641 (Oct. 2013).
- [24] Deledalle, C.-a., Denis, L., and Tupin, F., "NL-InSAR: Nonlocal Interferogram Estimation," *IEEE Transactions on Geoscience and Remote Sensing* **49**, 1441–1452 (Apr. 2011).
- [25] Garca-Ruiz, J.M. and Chueca, J. and Julin, A., "Los Movimientos en Masa del Alto Gallego," *Geografa Fsica de Aragn. Aspectos generales y temticos* , 142–152, (2004).
- [26] "Informe sobre las inestabilidades detectadas en una ladera en las inmediaciones del Puerto de Portalet (Sallent de Gallego, Huesca), donde se est ejecutando la construccin de un futuro aparcamiento," tech. rep., Ilustre Colegio Oficial de Geologos de Aragon (2005).

- [27] Herrera, G., Fernandez-Merodo, J., Mulas, J., Pastor, M., Luzi, G., and Monserrat, O., “A landslide forecasting model using ground based SAR data: The Portalet case study,” *Engineering Geology* **105**, 220–230 (May 2009).
- [28] Cooksley, G., Sanchez, F., Sabater, J., and Banwell, M., “Ground motion detection using radar satellites in areas prone to landslides: El Portalet landslide and Valle de Tena, Spain.,” in [*11th International Symposium on Landslides and 2nd North American Symposium on Landslides*], **2**(2), 1339–1344, CRC Press (2011).
- [29] Fernández-Merodo, J. a., García-Davalillo, J. C., Herrera, G., Mira, P., and Pastor, M., “2D viscoplastic finite element modelling of slow landslides: the Portalet case study (Spain),” *Landslides* **11**, 29–42 (Dec. 2012).
- [30] Manconi, A. and Giordan, D., “Surface displacements following the Mw 6.3 L’Aquila earthquake: One year of continuous monitoring via Robotized Total Station,” *Italian Journal of ...* **131**(3), 403–409 (2012).
- [31] Allasia, P., Manconi, A., Giordan, D., Baldo, M., and Lollino, G., “ADVICE: a new approach for near-real-time monitoring of surface displacements in landslide hazard scenarios.,” *Sensors (Basel, Switzerland)* **13**, 8285–302 (Jan. 2013).
- [32] Lollino, G., Arattano, M., Allasia, P., and Giordan, D., “Time response of a landslide to meteorological events,” *Natural Hazards and Earth System Sciences* **6**(September 2000), 179–184 (2006).
- [33] Seymour, M. and Cumming, I., “Maximum likelihood estimation for SAR interferometry,” in [*Proceedings of IGARSS ’94 - 1994 IEEE International Geoscience and Remote Sensing Symposium*], **4**, 2272–2275, IEEE (1994).